Eur. Phys. J. C 52, 383–395 (2007)
DOI 10.1140/epjc/s10052-007-0398-0

THE EUROPEAN PHYSICAL JOURNAL C

Regular Article – Theoretical Physics

Search for heavy neutral MSSM Higgs bosons with CMS: reach and Higgs mass precision

S. Gennai[1,a], S. Heinemeyer[2,b], A. Kalinowski[3,c], R. Kinnunen[4,d], S. Lehti[4,e], A. Nikitenko[5,f], G. Weiglein[6,g]

[1] Centro Studi Enrico Fermi, Rome and INFN Pisa, Italy
[2] Instituto de Fisica de Cantabria IFCA (CSIC-UC), Edificio Juan Jorda, Avda. de Los Castros s/n, 39005 Santander, Spain
[3] Institute of Experimental Physics, Warsaw, Poland
[4] Helsinki Institute of Physics, Helsinki, Finland
[5] Imperial College, London, UK; on leave from ITEP, Moscow, Russia
[6] IPPP, University of Durham, Durham DH1 3LE, UK

Received: 2 May 2007 /
Published online: 5 September 2007 –

Abstract. The search for MSSM Higgs bosons will be an important goal at the LHC. We analyze the search reach of the CMS experiment for the heavy neutral MSSM Higgs bosons with an integrated luminosity of 30 or 60 fb^{-1}. This is done by combining the latest results for the CMS experimental sensitivities based on full simulation studies with state-of-the-art theoretical predictions of the MSSM Higgs-boson properties. The results are interpreted in MSSM benchmark scenarios in terms of the parameters $\tan\beta$ and the Higgs-boson mass scale, M_A. We study the dependence of the 5σ discovery contours in the M_A–$\tan\beta$ plane on variations of the other supersymmetric parameters. The largest effects arise from a change in the higgsino mass parameter μ, which enters both via higher-order radiative corrections and via the kinematics of Higgs decays into supersymmetric particles. While the variation of μ can shift the prospective discovery reach (and correspondingly the "LHC wedge" region) by about $\Delta\tan\beta = 10$, we find that the discovery reach is rather stable with respect to the impact of other supersymmetric parameters. Within the discovery region we analyze the accuracy with which the masses of the heavy neutral Higgs bosons can be determined. We find that an accuracy of 1%–4% should be achievable, which could make it possible in favorable regions of the MSSM parameter space to experimentally resolve the signals of the two heavy MSSM Higgs bosons at the LHC.

1 Introduction

Identifying the mechanism of electroweak symmetry breaking will be one of the main goals of the LHC. Many possibilities have been studied in the literature, of which the most popular ones are the Higgs mechanism within the standard model (SM) and within the minimal supersymmetric standard model (MSSM) [1–3]. Contrary to the case of the SM, in the MSSM two Higgs doublets are required. This results in five physical Higgs bosons instead of the single Higgs boson of the SM. These are the light and heavy $\mathcal{CP}$-even Higgs bosons, h and H, the $\mathcal{CP}$-odd Higgs boson, A, and the charged Higgs boson, $H^\pm$.[1] The Higgs sector of the MSSM can be specified at lowest order in terms of the gauge couplings, the ratio of the two Higgs vacuum expectation values, $\tan\beta \equiv v_2/v_1$, and the mass of the $\mathcal{CP}$-odd Higgs boson, M_A. Consequently, the masses of the $\mathcal{CP}$-even neutral Higgs bosons and the charged Higgs boson are dependent quantities that can be predicted in terms of the Higgs-sector parameters. Higgs phenomenology in the MSSM is strongly affected by higher-order corrections, in particular from the sector of the third generation quarks and squarks, so that the dependencies on various other MSSM parameters can be important.

After the termination of LEP in the year 2000 (the final LEP results can be found in [4, 5]), and the (ongoing) Higgs-boson search at the Tevatron [6–12], the search will be continued at the LHC [13–15] (see also [16, 17] for recent reviews). The current exclusion bounds within the MSSM [5–10] and the prospective sensitivities at the LHC are usually displayed in terms of the parameters M_A and $\tan\beta$ that characterize the MSSM Higgs sector at lowest order. The other MSSM parameters are conventionally fixed according to certain benchmark scenarios [18–20]. The most prominent one is the "$m_h^{\max}$ scenario", which in the search for the light $\mathcal{CP}$-even Higgs boson allows one

[a] e-mail: Simone.Gennai@cern.ch
[b] e-mail: Sven.Heinemeyer@cern.ch
[c] e-mail: Artur.Kalinowski@cern.ch
[d] e-mail: Ritva.Kinnunen@cern.ch
[e] e-mail: Sami.Lehti@cern.ch
[f] e-mail: Alexandre.Nikitenko@cern.ch
[g] e-mail: Georg.Weiglein@durham.ac.uk

[1] We focus in this paper on the case without explicit $\mathcal{CP}$-violation in the soft supersymmetry-breaking terms.

to obtain conservative bounds on $\tan\beta$ for fixed values of the top-quark mass and the scale of the supersymmetric particles [21]. Besides the "no-mixing scenario", which is similar to the $m_h^{\max}$ scenario but assumes vanishing mixing in the stop sector, other $\mathcal{CP}$-conserving scenarios that have been studied in LHC analyses (see e.g. [17]) are the "gluophobic Higgs scenario" and the "small $\alpha_{\rm eff}$" scenario [19].

For the interpretation of the exclusion bounds and prospective discovery contours in the benchmark scenarios it is important to assess how sensitively the results depend on those parameters that have been fixed according to the benchmark prescriptions. While in the decoupling limit, which is the region of MSSM parameter space with $M_A \gg M_Z$, the couplings of the light $\mathcal{CP}$-even Higgs boson approach those of a SM Higgs boson with the same mass, the couplings of the heavy Higgs bosons of the MSSM can be sizably affected by higher-order contributions even for large values of M_A. The kinematics of the heavy Higgs-boson production processes, on the other hand, is governed by the parameter M_A, since in the region of large M_A the heavy MSSM Higgs bosons are nearly mass-degenerate, $M_A \approx M_H \approx M_{H^\pm}$. In [20] it has been shown that higher-order contributions to the relation between the bottom-quark mass and the bottom Yukawa coupling have a dramatic effect on the exclusion bounds in the M_A–$\tan\beta$ plane obtained from the $b\bar{b}\phi, \phi \to b\bar{b}$ channel at the Tevatron.

In this article we investigate how the 5σ discovery regions in the M_A–$\tan\beta$ plane for the heavy neutral MSSM Higgs bosons (a corresponding analysis for the charged Higgs-boson search will be presented elsewhere) obtainable with the CMS experiment at the LHC depend on the other MSSM parameters. For the experimental sensitivities achievable with CMS we use up-to-date results based on full simulation studies for 30 or 60 fb^{-1} (depending on the channel) [15]. This information is combined with precise theory predictions for the Higgs-boson masses and the involved production and decay processes incorporating higher-order corrections at the one-loop and two-loop level. In our analysis we investigate the impact on the discovery reach arising both from higher-order corrections and from possible decays of the heavy Higgs bosons into supersymmetric particles.[2]

The search for the heavy neutral MSSM Higgs bosons at the LHC will mainly be pursued in the b quark associated production with a subsequent decay to τ leptons [13–15]. In the region of large $\tan\beta$ this production process benefits from an enhancement factor of $\tan^2\beta$ compared to the SM case. The main search channels are[3] (here and in the following ϕ denotes the two heavy neutral MSSM Higgs bosons, $\phi = H, A$):

$$b\bar{b}\phi, \phi \to \tau^+\tau^- \to 2\mathrm{jets}\,, \tag{1}$$

$$b\bar{b}\phi, \phi \to \tau^+\tau^- \to \mu + \mathrm{jet}\,, \tag{2}$$

$$b\bar{b}\phi, \phi \to \tau^+\tau^- \to e + \mathrm{jet}\,, \tag{3}$$

$$b\bar{b}\phi, \phi \to \tau^+\tau^- \to e + \mu\,. \tag{4}$$

For our numerical analysis we use the program FeynHiggs [29–33]. We study in particular the dependence of the "LHC wedge" region, i.e. the region in which only the light $\mathcal{CP}$-even MSSM Higgs boson can be detected at the LHC at the 5σ level, on the variation of the higgsino mass parameter μ. The dependence on μ enters in two different ways, on the one hand via higher-order corrections affecting the relation between the bottom mass and the bottom Yukawa coupling, and on the other hand via the kinematics of Higgs decays into supersymmetric particles. We analyze both effects separately and discuss the possible impact of other supersymmetric parameters.

Our results for the discovery reach of the heavy neutral MSSM Higgs bosons extend the known results in the literature in various ways. In comparison with [34, 35], where the prospective 5σ discovery contours for CMS in the M_A–$\tan\beta$ plane of the $m_h^{\max}$ benchmark scenario were given for three different values of μ, the results in the present paper are based on full simulation studies and make use of the most up-to-date CMS tools for triggering and event reconstruction. Furthermore, in the analysis of [34, 35] relevant higher-order corrections, in particular those depending on Δ_b (see Sect. 2.2 below), have been neglected. The effects induced by the Δ_b corrections have been investigated in [20], where the results were obtained by a simple rescaling of the experimental results given in [13, 34–37]. Our present analysis, on the other hand, makes use of the latest CMS studies and provides a separate treatment of the different τ final states, channels (1)–(4).

As a second step of our analysis we investigate the experimental precision that can be achieved for the determination of the heavy Higgs-boson masses in the discovery channels (1)–(4). We discuss the prospective accuracy of the mass measurement in view of the possibility to experimentally resolve the signals of the heavy neutral MSSM Higgs bosons.

The paper is organized as follows: Sect. 2 introduces our notation and gives a brief summary of the most relevant supersymmetric radiative corrections to the Higgs-boson masses, production cross sections and decay widths at the LHC. The relevant benchmark scenarios are briefly reviewed. In Sect. 3 the experimental analysis is described. The results for the variation of the 5σ discovery contours, obtainable at CMS with 30 or 60 fb^{-1} are given in Sect. 4, where we also discuss the achievable experimental precision in the Higgs mass determination. The conclusions can be found in Sect. 5.

2 Phenomenology of the MSSM Higgs sector

2.1 Notation

The MSSM Higgs sector at lowest order is described in terms of two independent parameters (besides the SM

[2] We restrict our analysis to the impact of supersymmetric contributions. For a discussion of uncertainties related to parton distribution functions, see e.g. [22].

[3] In our analysis we do not consider diffractive Higgs production, $pp \to p \oplus H \oplus p$ [23–27]. For a detailed discussion of the search reach for the heavy neutral MSSM Higgs bosons in diffractive Higgs production we refer to [28].

gauge couplings): $\tan\beta \equiv v_2/v_1$, the ratio of the two vacuum expectation values, and M_A, the mass of the $\mathcal{CP}$-odd Higgs boson A. Beyond the tree level, large radiative corrections can occur from the $t/\tilde{t}$ sector, and for large values of $\tan\beta$ also from the $b/\tilde{b}$ sector.

Our notations for the scalar top and scalar bottom sector of the MSSM are as follows: the mass matrices in the basis of the current eigenstates $\tilde{t}_\mathrm{L}, \tilde{t}_\mathrm{R}$ and $\tilde{b}_\mathrm{L}, \tilde{b}_\mathrm{R}$ are given by

$$\mathcal{M}^2_{\tilde{t}} = \begin{pmatrix} M^2_{\tilde{Q}} + m_t^2 + \cos 2\beta \left(\frac{1}{2} - \frac{2}{3}s^2_\mathrm{W}\right) M_Z^2 & m_t X_t \\ m_t X_t & M^2_{\tilde{t}_R} + m_t^2 + \frac{2}{3}\cos 2\beta s^2_\mathrm{W} M_Z^2 \end{pmatrix}, \tag{5}$$

$$\mathcal{M}^2_{\tilde{b}} = \begin{pmatrix} M^2_{\tilde{Q}} + m_b^2 + \cos 2\beta(-\frac{1}{2} + \frac{1}{3}s^2_\mathrm{W}) M_Z^2 & m_b X_b \\ m_b X_b & M^2_{\tilde{b}_R} + m_b^2 - \frac{1}{3}\cos 2\beta s^2_\mathrm{W} M_Z^2 \end{pmatrix}, \tag{6}$$

where

$$\begin{aligned} m_t X_t &= m_t(A_t - \mu \cot\beta\,)\,, \\ m_b\, X_b &= m_b\,(A_b - \mu \tan\beta\,)\,. \end{aligned} \tag{7}$$

Here $M_{\tilde{Q}}$, $M_{\tilde{t}_R}$ and $M_{\tilde{b}_R}$ are the diagonal soft SUSY-breaking parameters, A_t denotes the trilinear Higgs–stop coupling, A_b denotes the Higgs–sbottom coupling, and μ is the higgsino mass parameter.

For the numerical evaluation, it is often convenient to choose

$$M_{\tilde{Q}} = M_{\tilde{t}_R} = M_{\tilde{b}_R} =: M_\mathrm{SUSY}\,. \tag{8}$$

Concerning analyses for the case where $M_{\tilde{t}_R} \neq M_{\tilde{Q}} \neq M_{\tilde{b}_R}$, see e.g. [31, 38, 39]. It has been shown that the upper bound on the mass of the light $\mathcal{CP}$-even Higgs boson, M_h, obtained using (8) is the same as for the more general case, provided that M_SUSY is identified with the heaviest mass of $M_{\tilde{Q}}$, $M_{\tilde{t}_R}$ and $M_{\tilde{b}_R}$ [31].

Accordingly, the most important parameters entering the Higgs-sector predictions via higher-order corrections are m_t, M_SUSY, X_t, X_b and μ (see also the discussion in Sect. 2.2.2 below). The Higgs-sector observables furthermore depend on the SU(2) gaugino mass parameter, M_2, the U(1) parameter M_1 and the gluino mass, $m_{\tilde{g}}$ (the latter enters the predictions for the Higgs-boson masses only from two-loop order on). In numerical analyses the U(1) gaugino mass parameter, M_1, is often fixed via the GUT relation

$$M_1 = \frac{5}{3}\frac{s^2_\mathrm{W}}{c^2_\mathrm{W}} M_2\,. \tag{9}$$

We will briefly comment below on the possible impact of complex phases entering the Higgs-sector predictions via higher-order contributions.

2.2 Higher-order corrections in the Higgs sector

In the following we briefly summarize the most important higher-order corrections affecting the observables in the MSSM Higgs-boson sector. As mentioned above, we focus on the MSSM with real parameters. For our numerical analysis we use the program FeynHiggs [29–33][4], which incorporates a comprehensive set of higher-order results, obtained in the Feynman-diagrammatic approach [31–33, 40–43].

2.2.1 Higgs-boson propagator corrections

Higher-order corrections to the Higgs-boson masses and the wave function normalization factors of processes with external Higgs bosons arise from Higgs-boson propagator-type contributions. These corrections furthermore contribute in a universal way to all Higgs-boson couplings. For the propagator-type corrections in the MSSM the complete one-loop results [44–51], the bulk of the two-loop contributions [31, 39–42, 52–78] and even leading three-loop corrections [79] are known. The remaining theoretical uncertainty on the light $\mathcal{CP}$-even Higgs-boson mass has been estimated to be below $\sim 3\,\mathrm{GeV}$ [32, 80]. The by far dominant contribution is the $\mathcal{O}(\alpha_t)$ term due to top and stop loops ($\alpha_t \equiv h_t^2/(4\pi)$, where h_t denotes the top-quark Yukawa coupling). Effects of $\mathcal{O}(\alpha_b)$ can be important for large values of $\tan\beta$.

2.2.2 Corrections to the relation between the bottom-quark mass and the bottom Yukawa coupling

Concerning the corrections from the bottom/sbottom sector, large higher-order effects can in particular occur in the relation between the bottom-quark mass and the bottom Yukawa coupling (which controls the interaction between the Higgs bosons and bottom quarks as well as between the Higgs and scalar bottoms), h_b, for large values of $\tan\beta$. At lowest order the relation reads $m_b = h_b v_1$. Beyond the tree level large radiative corrections proportional to $h_b v_2$ are induced, giving rise to $\tan\beta$-enhanced contributions [66–70, 81]. At the one-loop level the leading terms proportional to v_2 are generated either by gluino–sbottom one-loop diagrams of $\mathcal{O}(\alpha_s)$ or by chargino–stop loops of $\mathcal{O}(\alpha_t)$.

The leading one-loop contribution Δ_b in the limit of $M_\mathrm{SUSY} \gg m_t$ and $\tan\beta \gg 1$ takes the simple form [66–68]

$$\begin{aligned} \Delta_b = {} & \frac{2\alpha_s}{3\pi} m_{\tilde{g}} \mu \tan\beta \times I(m_{\tilde{b}_1}, m_{\tilde{b}_2}, m_{\tilde{g}}) \\ & + \frac{\alpha_t}{4\pi} A_t \mu \tan\beta I(m_{\tilde{t}_1}, m_{\tilde{t}_2}, \mu)\,, \end{aligned} \tag{10}$$

where the function I is given by

$$\begin{aligned} I(a,b,c) = {} & \frac{1}{(a^2-b^2)(b^2-c^2)(a^2-c^2)} \\ & \times \left(a^2 b^2 \log\frac{a^2}{b^2} + b^2 c^2 \log\frac{b^2}{c^2} + c^2 a^2 \log\frac{c^2}{a^2} \right) \end{aligned}$$

[4] The code can be obtained from www.feynhiggs.de.

$$\sim \frac{1}{\max(a^2, b^2, c^2)}\,. \tag{11}$$

The leading contribution can be resummed to all orders in the perturbative expansion [66–70]. This leads in particular to the replacement

$$\overline{m}_b \to \frac{\overline{m}_b}{1+\Delta_b}, \tag{12}$$

where $\overline{m}_b$ denotes the running bottom quark mass including SM QCD corrections. For the numerical evaluations in this paper we choose $\overline{m}_b = \overline{m}_b(m_t) \approx 2.97\,\text{GeV}$.

The Δ_b corrections are numerically sizable for large $\tan\beta$ in combination with large values of the ratios of $\mu m_{\tilde{g}}/M^2_{\text{SUSY}}$ or $\mu A_t/M^2_{\text{SUSY}}$. Negative values of Δ_b lead to an enhancement of the bottom Yukawa coupling as a consequence of (12) (for extreme values of μ and $\tan\beta$ the bottom Yukawa coupling can even acquire non-perturbative values when $\Delta_b \to -1$), while positive values of Δ_b give rise to a suppression of the Yukawa coupling. Since a change in the sign of μ reverses the sign of Δ_b, the bottom Yukawa coupling can exhibit a very pronounced dependence on the parameter μ.

For large values of $\tan\beta$ the correction to the production cross sections of the Higgs bosons H and A induced by Δ_b enters approximately like $\tan^2\beta/(1+\Delta_b)^2$, giving rise to potentially large numerical effects. In the case of the subsequent Higgs-boson decay $\phi \to \tau^+\tau^-$, however, the Δ_b corrections in the production and the decay process cancel each other to a large extent. The residual Δ_b dependence of $\sigma(b\bar{b}\phi) \times \text{BR}(\phi \to \tau^+\tau^-)$ is approximately given by $\tan^2\beta/((1+\Delta_b)^2+9)$, which has a much weaker Δ_b dependence (see [20] for a more detailed discussion).

In the numerical analysis below the Δ_b corrections, which have been discussed in this section in terms of simple approximation formulae, will be supplemented by other higher-order corrections as implemented in the program FeynHiggs (and possible decay modes into supersymmetric particles are taken into account). Higher-order corrections to Higgs decays into $\tau^+\tau^-$ within the SM and MSSM have been evaluated in [50, 51, 82–91].

2.2.3 Corrections to the Higgs production cross sections

For the prediction of Higgs-boson production processes at hadron colliders SM-type QCD corrections in general play an important role. The SM predictions for the process $b\bar{b} \to \phi + X$ at the LHC are far advanced. In the five-flavor scheme the SM cross section is known at NNLO in QCD [92]. The cross section in the four-flavor scheme is known at NLO [93, 94]. Results obtained in the two schemes have been shown to be consistent [95–97] (see also [96, 98] and [93, 94] for results with one and two final-state b-quarks at high p_T, respectively).

The predictions for the $b\bar{b} \to \phi + X$ cross sections in the MSSM have been obtained with FeynHiggs [29–33]. The FeynHiggs implementation[5] is based on the state-of-the-art SM prediction, namely the NNLO result in the five-flavor scheme [92] using MRST2002 parton distributions at NNLO [99], with the renormalization scale set equal to $M_{H^{\text{SM}}}$ and the factorization scale set equal to $M_{H^{\text{SM}}}/4$. In order to obtain the MSSM prediction the SM cross section is rescaled with the ratio of the partial widths in the MSSM and the SM,

$$\frac{\Gamma(\phi \to b\bar{b})_{\text{MSSM}}}{\Gamma(\phi \to b\bar{b})_{\text{SM}}}\,. \tag{13}$$

The evaluation of the partial widths incorporates one-loop SM QCD and SUSY QCD corrections, as well as (in the SUSY case) the resummation of all terms of $\mathcal{O}((\alpha_s \tan\beta)^n)$ [50, 51, 69, 82–91] and the proper normalization of the external Higgs bosons as discussed in [33, 100]. Since the approximation of rescaling the SM cross section with the ratio of partial widths does not take into account the MSSM-specific dynamics of the production processes, the theoretical uncertainty in the predictions for the cross sections will in general be somewhat larger than for the decay widths. It should be noted that in comparison with other approaches for treating the SM and SUSY contributions, for instance the program HQQ [101], sizable deviations can occur as a consequence of differences in the scale choices and the inclusion of higher-order corrections.

2.3 The m_h^{max} and no-mixing benchmark scenarios

While the phenomenology of the production and decay processes of the heavy neutral MSSM Higgs bosons at the LHC is mainly characterized by the parameters M_A and $\tan\beta$ that govern the Higgs sector at lowest order, other MSSM parameters enter via higher-order contributions, as discussed above, and via the kinematics of Higgs-boson decays into supersymmetric particles. The other MSSM parameters are usually fixed in terms of benchmark scenarios. The most commonly used scenarios are the "m_h^{max}" and "no-mixing" benchmark scenarios [18–20]. According to the definition of [19] the m_h^{max} scenario is given by

$$\begin{aligned} &M_{\text{SUSY}} = 1000\,\text{GeV}\,, \quad X_t = 2\,M_{\text{SUSY}}\,, \quad A_b = A_t\,, \\ &\mu = 200\,\text{GeV}\,, \quad M_2 = 200\,\text{GeV}\,, \\ &m_{\tilde{g}} = 0.8\,M_{\text{SUSY}}\,. \end{aligned} \tag{14}$$

The no-mixing scenario differs from the m_h^{max} scenario only in that it has vanishing mixing in the stop sector and a larger value of M_{SUSY}:

$$\begin{aligned} &M_{\text{SUSY}} = 2000\,\text{GeV}\,, \quad X_t = 0\,, \quad A_b = A_t\,, \\ &\mu = 200\,\text{GeV}\,, \quad M_2 = 200\,\text{GeV}\,, \\ &m_{\tilde{g}} = 0.8\,M_{\text{SUSY}}\,. \end{aligned} \tag{15}$$

The value of the top-quark mass in [19] was chosen according to the experimental central value at that time. For our numerical analysis below, we use the value, $m_t = 171.4\,\text{GeV}$ [102][6].

[5] The inclusion of the charged Higgs production cross sections is planned for the near future.

[6] Most recently the central experimental value has shifted to $m_t = 170.9 \pm 1.8\,\text{GeV}$ [103]. This shift has a negligible impact on our analysis.

In [20] it was suggested that in the search for heavy MSSM Higgs bosons the $m_h^{\max}$ and no-mixing scenarios, which originally were mainly designed for the search for the light $\mathcal{CP}$-even Higgs boson h, should be extended by several discrete values of μ,

$$\mu = \pm 200\,, \pm 500\,, \pm 1000\,\text{GeV}\,. \tag{16}$$

As discussed above, the variation of μ in particular has an impact on the correction Δ_b, modifying in this way the bottom Yukawa coupling. For very large values of $\tan\beta$ and large negative values of μ the bottom Yukawa coupling can be so much enhanced that a perturbative treatment is no longer possible. We have checked that in our analysis of the LHC discovery contours the bottom Yukawa coupling stays in the perturbative regime, so that all values of μ down to $\mu = -1000\,\text{GeV}$ can safely be inserted.

The variation of the parameter μ also modifies the mass spectrum and the couplings in the chargino and neutralino sector of the MSSM. Besides the small higher-order corrections induced by loop diagrams involving charginos and neutralinos, a change in the mass spectrum of the chargino and neutralino sector can have an important effect on Higgs phenomenology because decay modes of the heavy neutral MSSM Higgs bosons into charginos and neutralinos open up if the supersymmetric particles are sufficiently light (the mass spectrum in the $m_h^{\max}$ and no-mixing scenarios respects the limits from direct searches for charginos at LEP [104] for all values of μ specified in (16)).

Differences between the $m_h^{\max}$ and no-mixing scenarios in the searches for heavy neutral MSSM Higgs bosons are induced in particular by a difference in the Δ_b correction. While in the $m_h^{\max}$ scenario both the $\mathcal{O}(\alpha_s)$ and $\mathcal{O}(\alpha_t)$ contributions to Δ_b can be sizable, see (10), in the no-mixing scenario the $\mathcal{O}(\alpha_t)$ contribution is very small because A_t is close to zero in this case. The larger value of M_{SUSY} in the no-mixing scenario gives rise to an additional suppression of $|\Delta_b|$ compared to the $m_h^{\max}$ scenario.

3 Experimental analysis

In this section we briefly review the recent CMS analysis of the $\phi \to \tau^+\tau^-$ channel, see [15], yielding the number of events needed for a 5σ discovery (depending on the mass of the Higgs boson). The analysis was performed with full CMS detector simulation and reconstruction for the following four final states of di-τ-lepton decays: $\tau^+\tau^- \to$ jets [105], $\tau^+\tau^- \to e +$ jet [106], $\tau^+\tau^- \to \mu +$ jet [107] and $\tau^+\tau^- \to e + \mu$ [108].

The Higgs-boson production in association with b quarks, $pp \to b\bar{b}\phi$, has been selected using single b-jet tagging in the experimental analysis. The kinematics of the $gg \to b\bar{b}\phi$ production process ($2 \to 3$) was generated with PYTHIA [109]. It has been shown that in this way the NLO kinematics is better reproduced than using the PYTHIA $gb \to b\phi$ process ($2 \to 2$) [110]. The backgrounds considered in the analysis were QCD muli-jet events (for the $\tau\tau \to$ jets mode), $t\bar{t}, b\bar{b}$, Drell–Yan production of Z, γ^*, $W +$ jet, Wt and $\tau\tau b\bar{b}$. All background processes were generated using PYTHIA, except for $\tau^+\tau^- b\bar{b}$, which was generated using CompHEP [111].

The results for the various channels, (1)–(4), are given in Tables 1–4. For every Higgs-boson mass point studied we show the number of signal events needed for 5σ discovery, N_S, the total experimental selection efficiency, ε_{exp},

Table 1. Required number of signal events, N_S, with $\mathcal{L} = 60\,\text{fb}^{-1}$ for a 5σ discovery in the channel $\phi \to \tau^+\tau^- \to$ jets. Furthermore we give the total experimental selection efficiency, ε_{exp}, the ratio of the di-τ mass resolution to the Higgs-boson mass, R_{M_ϕ}, and the expected precision of the Higgs-boson mass measurement, $\Delta M_\phi / M_\phi$, obtainable from N_S signal events

$\phi \to \tau^+\tau^- \to$ jets, $60\,\text{fb}^{-1}$			
M_A [GeV]	200	500	800
N_S	63	35	17
ε_{exp}	2.5×10^{-4}	2.4×10^{-3}	3.6×10^{-3}
R_{M_ϕ}	0.176	0.171	0.187
$\Delta M_\phi / M_\phi$ [%]	2.2	2.8	4.5

Table 2. Required number of signal events, N_S, with $\mathcal{L} = 30\,\text{fb}^{-1}$ for a 5σ discovery in the channel $\phi \to \tau^+\tau^- \to e +$ jet. The other quantities are defined as in Table 1

$\phi \to \tau^+\tau^- \to e +$ jet, $30\,\text{fb}^{-1}$			
M_A [GeV]	200	300	500
N_S	72.9	45.5	32.8
ε_{exp}	3.0×10^{-3}	6.4×10^{-3}	1.0×10^{-2}
R_{M_ϕ}	0.216	0.214	0.230
$\Delta M_\phi / M_\phi$ [%]	2.5	3.2	4.0

Table 3. Required number of signal events, N_S, with $\mathcal{L} = 30\,\text{fb}^{-1}$ for a 5σ discovery in the channel $\phi \to \tau^+\tau^- \to \mu +$ jet. The other quantities are defined as in Table 1

$\phi \to \tau^+\tau^- \to \mu +$ jet, $30\,\text{fb}^{-1}$		
M_A [GeV]	200	500
N_S	79	57
ε_{exp}	7.0×10^{-3}	2.0×10^{-2}
R_{M_ϕ}	0.210	0.200
$\Delta M_\phi / M_\phi$ [%]	2.4	2.6

Table 4. Required number of signal events, N_S, with $\mathcal{L} = 30\,\text{fb}^{-1}$ for a 5σ discovery in the channel $\phi \to \tau^+\tau^- \to e + \mu$. The other quantities are defined as in Table 1

$\phi \to \tau^+\tau^- \to e + \mu$, $30\,\text{fb}^{-1}$		
M_A [GeV]	200	250
N_S	87.8	136.7
ε_{exp}	6.4×10^{-3}	1.1×10^{-2}
R_{M_ϕ}	0.262	0.412
$\Delta M_\phi / M_\phi$ [%]	2.8	3.5

and the ratio of the di-τ mass resolution to the Higgs-boson mass, R_{M_ϕ}. The last row in Tables 1–4 shows the expected precision of the Higgs-boson mass measurement, evaluated as explained below, for parameter points on the 5σ discovery contour. Detector effects, experimental systematics and uncertainties of the background determination were taken into account in the evaluation of the N_S. These effects reduce the discovery region in the M_A–$\tan\beta$ plane as shown in previous analyses [15] (see in particular Fig. 5.6 of [15] for the $\tau^+\tau^- \to \mu + \text{jet}$ mode).

Now we turn to the evaluation of the expected precision of the Higgs-boson mass measurement. In spite of the escaping neutrinos, the Higgs-boson mass can be reconstructed in the $H, A \to \tau\tau$ channel from the visible τ momenta (τ jets) and the missing transverse energy, $E_{\mathrm{T}}^{\mathrm{miss}}$, using the collinearity approximation for neutrinos from highly boosted τ. In the investigated region of M_A and $\tan\beta$ the two states A and H are nearly mass-degenerate. For most values of the other MSSM parameters the mass difference of A and H is much smaller than the achievable mass resolution. In this case the difference in reconstructing the A or the H will have no relevant effect on the achievable accuracy in the mass determination. In some regions of the MSSM parameter space, however, a sizable splitting between M_A and M_H can occur even for $M_A \gg M_Z$. We will discuss below the prospects in scenarios where the splitting between M_A and M_H is relatively large. The precision $\Delta M_\phi / M_\phi$ shown in Tables 1–4 is derived for the border of the parameter space in which a 5σ discovery can be claimed, i.e. with N_S observed Higgs events. The statistical accuracy of the mass measurement has been evaluated via

$$\frac{\Delta M_\phi}{M_\phi} = \frac{R_{M_\phi}}{\sqrt{N_S}} \,. \tag{17}$$

A higher precision can be achieved if more than N_S events are observed. The corresponding estimate for the precision is obtained by replacing N_S in (17) by the number of observed signal events, N_{ev}. It should be noted that the prospective accuracy obtained from (17) does not take into account the uncertainties of the jet and missing E_{T} energy scales. In the $\tau^+\tau^- \to$ jets mode these effects can lead to an additional 3% uncertainty in the mass measurement [105]. A more dedicated procedure of the mass measurement from the signal plus background data still has to be developed in the experimental analysis. However, we do not expect that the additional uncertainties will considerably degrade the accuracy of the Higgs-boson mass measurement as calculated with (17).

4 Results

The results quoted in Sect. 3 for the required number of signal events depend only on the Higgs-boson mass, i.e. the event kinematics, but are independent of any specific MSSM scenario. In order to determine the 5σ discovery contours in the M_A–$\tan\beta$ plane these results have to be confronted with the MSSM predictions. The number of signal events, N_{ev}, for a given parameter point is evaluated via

$$N_{\mathrm{ev}} = \mathcal{L} \times \sigma_{b\bar{b}\phi} \times \mathrm{BR}(\phi \to \tau^+\tau^-) \times \mathrm{BR}_{\tau\tau} \times \varepsilon_{\mathrm{exp}} \,. \tag{18}$$

Here $\mathcal{L}$ denotes the luminosity collected with the CMS detector, $\sigma_{b\bar{b}\phi}$ is the Higgs-boson production cross section, $\mathrm{BR}(\phi \to \tau^+\tau^-)$ is the branching ratio of the Higgs boson to τ leptons, $\mathrm{BR}_{\tau\tau}$ is the product of the branching ratios of the two τ leptons into their respective final state,

$$\mathrm{BR}(\tau \to \mathrm{jet} + X) \approx 0.65 \,, \tag{19}$$

$$\mathrm{BR}(\tau \to \mu + X) \approx \mathrm{BR}(\tau \to e + X) \approx 0.175 \,, \tag{20}$$

and $\varepsilon_{\mathrm{exp}}$ denotes the total experimental selection efficiency for the respective process (as given in Tables 1–4). The Higgs-boson production cross sections and decay branching ratios have been evaluated with FeynHiggs as described in Sect. 2.2.

4.1 Discovery reach for heavy neutral MSSM Higgs bosons

The number of signal events, N_{ev}, in the MSSM depends besides the parameters M_A and $\tan\beta$, which govern the MSSM Higgs sector at lowest order, in principle also on all other MSSM parameters. In the following we analyze how stable the results for the 5σ discovery contours in the M_A–$\tan\beta$ plane are with respect to variations of the other MSSM parameters. We take into account both effects from higher-order corrections, as discussed in Sect. 2.2, and from decays of the heavy Higgs bosons into supersymmetric particles. As starting point of our analysis we use the m_h^{max} and no-mixing benchmark scenarios, where we investigate in detail the sensitivity of the discovery contours with respect to variations of the parameter μ. We then discuss the possible impact of varying other MSSM parameters.

We have evaluated N_{ev} in the two benchmark scenarios as a function of M_A and $\tan\beta$. For fixed M_A we have varied $\tan\beta$ such that $N_{\mathrm{ev}} = N_S$ (as given in Tables 1–4). This $\tan\beta$ value is then identified as the point on the 5σ discovery contour corresponding to the chosen value of M_A. In this way we have determined the 5σ discovery contours for the m_h^{max} and the no-mixing scenarios for $\mu = \pm 200, \pm 1000\,\mathrm{GeV}$.

In Figs. 1–3 we show the 5σ discovery contours obtained from the process $b\bar{b}\phi, \phi \to \tau^+\tau^-$ for the final states $\tau^+\tau^- \to$ jets, $\tau^+\tau^- \to e +$ jet and $\tau^+\tau^- \to \mu +$ jet. As can be seen from Table 4, the fourth channel discussed above, $\tau^+\tau^- \to e + \mu$, contributes for $30\,\mathrm{fb}^{-1}$ only in the region of relatively small M_A values and has a lower sensitivity than the other three channels. We therefore omit this channel in the following discussion. The discovery contours in Figs. 1–3 are given for the m_h^{max} and no-mixing benchmark scenarios with $\mu = \pm 200, \pm 1000\,\mathrm{GeV}$. As explained above, the 5σ discovery contours are affected by a change in μ in two ways. Higher-order contribu-

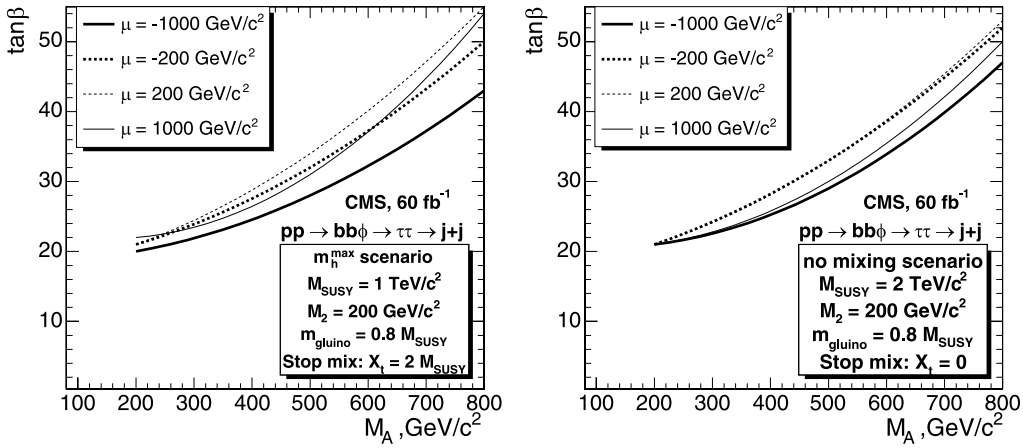

Fig. 1. Variation of the 5σ discovery contours obtained from the channel $b\bar{b}\phi, \phi \to \tau^+\tau^- \to$ jets in the $m_h^{\max}$ (*left*) and no-mixing (*right*) benchmark scenarios for different values of μ

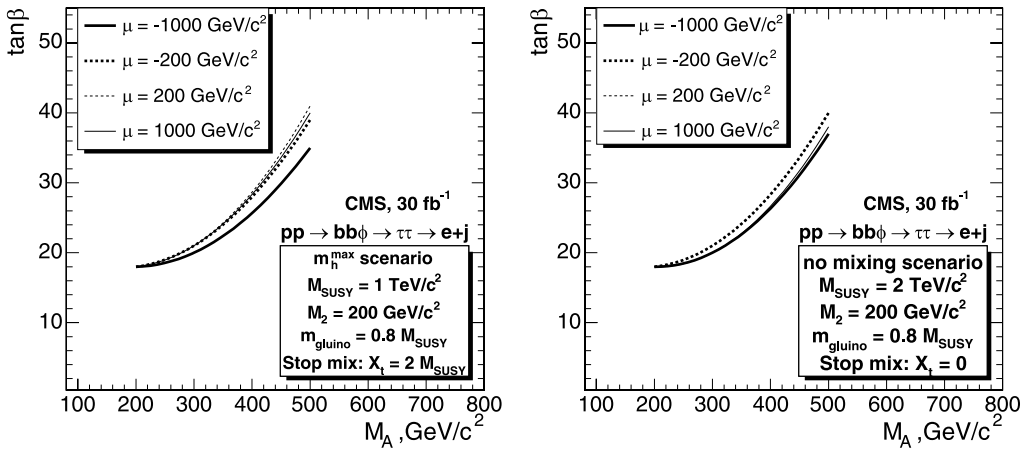

Fig. 2. Variation of the 5σ discovery contours obtained from the channel $b\bar{b}\phi, \phi \to \tau^+\tau^- \to e +$ jet in the $m_h^{\max}$ (*left*) and no-mixing (*right*) benchmark scenarios for different values of μ

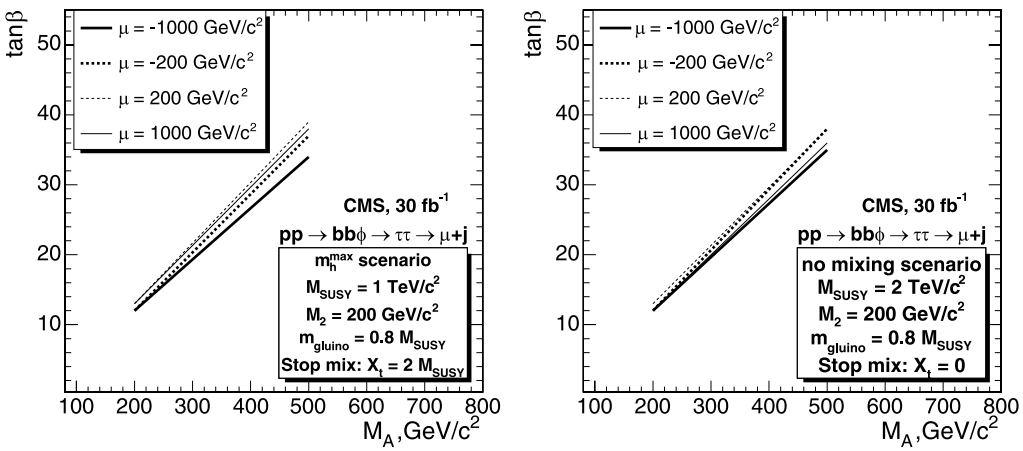

Fig. 3. Variation of the 5σ discovery contours obtained from the channel $b\bar{b}\phi, \phi \to \tau^+\tau^- \to \mu +$ jet in the $m_h^{\max}$ (*left*) and no-mixing (*right*) benchmark scenarios for different values of μ

tions, in particular the ones associated with Δ_b, modify the Higgs-boson production cross sections and decay branching ratios. Furthermore the mass eigenvalues of the charginos and neutralinos vary with μ, possibly opening up the decay channels of the Higgs bosons to supersymmetric particles, which reduces the branching ratio to τ leptons.

The results for the 5σ discovery contours for the final-state $\tau^+\tau^- \to$ jets are shown in Fig. 1 for the $m_h^{\max}$ (left) and the no-mixing (right) scenario. As expected from the discussion of the Δ_b corrections in Sect. 2.2, the variation of the 5σ discovery contours with μ is more pronounced in the $m_h^{\max}$ scenario, where a shift up to $\Delta \tan\beta = 12$ can be observed for $M_A = 800\,\text{GeV}$. For low M_A values (corresponding also to lower $\tan\beta$ values on the discovery contours) the variation stays below $\Delta \tan\beta = 3$. In the no-mixing scenario the variation does not exceed $\Delta \tan\beta = 5$. The $\tau^+\tau^- \to$ jets channel has also been discussed in [20]. Our results, which are based on the latest CMS studies using full simulation [105], are qualitatively in good agree-

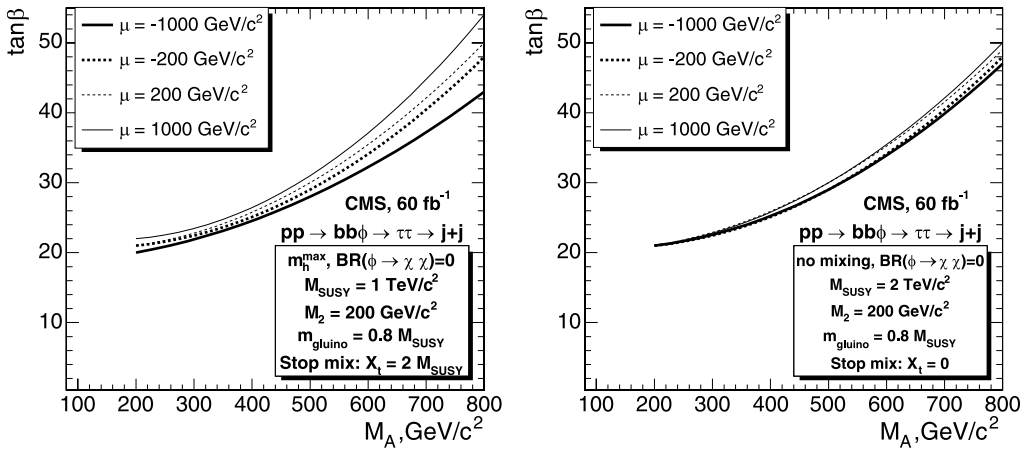

Fig. 4. Variation of the 5σ discovery contours obtained from the channel $b\bar{b}\phi, \phi \to \tau^+\tau^- \to$ jets in the $m_h^{\max}$ (*left*) and no-mixing (*right*) benchmark scenarios for different values of μ in the case where no decays of the heavy Higgs bosons into supersymmetric particles are taken into account (see text)

ment with [20], in which the earlier CMS studies of [34, 35] had beed used. The 5σ discovery regions are largest for $\mu = -1000\,\text{GeV}$ and pushed to highest $\tan\beta$ values for $\mu = +200\,\text{GeV}$. In the low M_A region our discovery contours are very similar to those obtained in [20]. In the high M_A region, $M_A \sim 800\,\text{GeV}$, corresponding to larger values of $\tan\beta$ on the discovery contours, our improved evaluation of the 5σ discovery contours gives rise to a shift towards higher $\tan\beta$ values compared to [20] of about $\Delta\tan\beta = 8$ (mostly due to the up-to-date experimental input). Accordingly, we find a smaller discovery region compared to [20] and therefore an enlarged "LHC wedge" region where only the light $\mathcal{CP}$-even MSSM Higgs boson can be detected at the 5σ level.

The results for the channel $\tau^+\tau^- \to e+\text{jet}$ are shown in Fig. 2. Again the $m_h^{\max}$ scenario shows a stronger variation than the no-mixing scenario. The resulting shift in $\tan\beta$ reaches up to $\Delta\tan\beta = 8$ for $M_A = 500\,\text{GeV}$ in the $m_h^{\max}$ scenario, but it stays below $\Delta\tan\beta = 4$ for the no-mixing scenario. Finally in Fig. 3 the results for the channel $\tau^+\tau^- \to \mu+\text{jet}$ are depicted. The level of variation of the 5σ discovery contours is the same as for the $e+\text{jet}$ final state.[7]

In order to gain a better understanding of how sensitively the discovery contours in the M_A–$\tan\beta$ plane depend on the chosen SUSY scenario, it is useful to separately investigate the different effects caused by varying the parameter μ. For simplicity, we restrict the following discussion to the $b\bar{b}\phi, \phi \to \tau^+\tau^- \to$ jets channel. In Fig. 4 we show the same results as in Fig. 1, but for the case where no decays of the heavy Higgs bosons into supersymmetric particles are taken into account. As a consequence, the variation of the 5σ discovery contours with μ shown in Fig. 4 is purely an effect of higher-order corrections, predominantly those entering via Δ_b. The difference between Fig. 1 and Fig. 4, on the other hand, is purely an effect of the change in $\text{BR}(\phi \to \tau^+\tau^-)$ caused by the variation of the partial Higgs-boson decay widths into supersymmetric particles arising from a shift in the masses of the charginos and neutralinos.

In Fig. 4 the dependence of the 5σ discovery contours on μ significantly differs from the case of Fig. 1. While in Fig. 1 the inclusion of decays into supersymmetric particles gives rise to the fact that the smallest discovery region is found for small μ values, $\mu = +200\,\text{GeV}$ (with the exception of the region of very small M_A), in Fig. 4 the 5σ discovery contours are ordered monotonously in μ: the largest (smallest) 5σ discovery regions are obtained for $\mu = -(+)1000\,\text{GeV}$, i.e. for the largest (smallest) values of the bottom Yukawa coupling. As expected, the effect of the higher-order corrections is largest in the high $\tan\beta$ region (corresponding to large values of M_A on the discovery contours). In this region the variation of μ shifts the discovery contours by up to $\Delta\tan\beta = 11$ for the case of the $m_h^{\max}$ scenario (left plot of Fig. 4), i.e. the effect is about the same as for the case where decays into supersymmetric particles are included. For lower values of $\tan\beta$ (corresponding to smaller values of M_A on the discovery contours), on the other hand, the modification of the Higgs branching ratio as a consequence of decays into supersymmetric particles yields the dominant effect on the 5σ discovery contours. Accordingly, the observed variation with μ in this region is significantly smaller in Fig. 4 as compared to the full result of Fig. 1. The reduced sensitivity of the discovery contours on μ can also clearly be seen for the case of the no-mixing scenario (right plot), where, as discussed above, the Δ_b correction is smaller than in the $m_h^{\max}$ scenario.

A parameter affecting the Δ_b corrections, see (10), but not the kinematics of the Higgs-boson decays is the gluino mass, $m_{\tilde{g}}$. We now investigate the impact of varying this parameter, which is normally fixed to the values $m_{\tilde{g}} = 800, 1600\,\text{GeV}$ in the $m_h^{\max}$ and no-mixing benchmark scenarios, respectively. The results for four different values of the gluino mass, $m_{\tilde{g}} = 200, 500, 1000, 2000\,\text{GeV}$, are shown in Fig. 5. The μ parameter has been set to $\mu = +1000\,\text{GeV}$ in Fig. 5, such that the Higgs decay channels into charginos and neutralinos are suppressed. As one can see from (10), the change of $m_{\tilde{g}}$ affects the $\mathcal{O}(\alpha_s)$ part of Δ_b and corresponds to a monotonous increase of Δ_b. As an example, this yields for $\mu = 1000\,\text{GeV}$, $\tan\beta = 50$ in the

[7] Since the results of the experimental simulation for this channel are available only for two M_A values, the interpolation is a straight line. This may result in a slightly larger uncertainty of the results shown in Fig. 3 compared to the other figures.

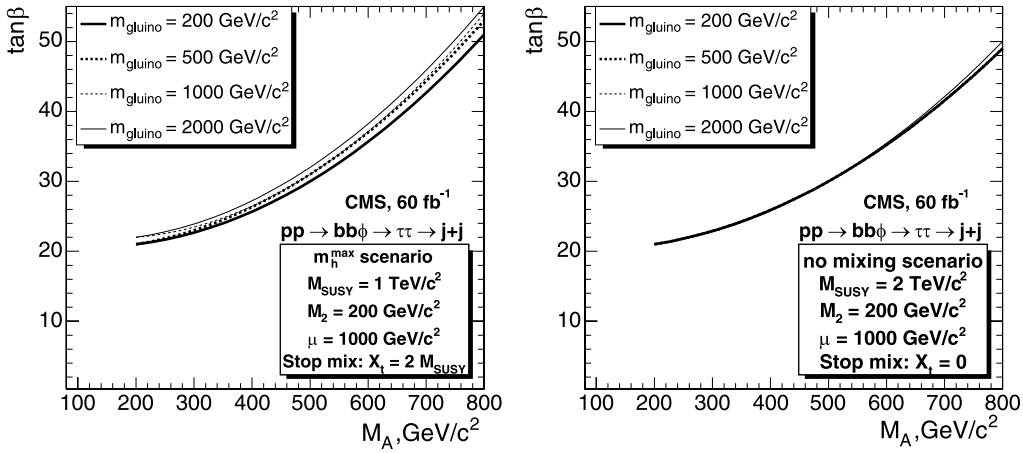

Fig. 5. Variation of the 5σ discovery contours obtained from the channel $b\bar{b}\phi, \phi \to \tau^+\tau^- \to$ jets in the $m_h^{\max}$ (*left*) and no-mixing (*right*) benchmark scenarios with $\mu = +1000\,\text{GeV}$ for different values of $m_{\tilde{g}}$

two scenarios:

$$\begin{aligned} m_h^{\max}, \quad & m_{\tilde{g}} = 200\,\text{GeV}: \quad \Delta_b = 0.50\,, \\ m_h^{\max}, \quad & m_{\tilde{g}} = 2000\,\text{GeV}: \quad \Delta_b = 0.94\,, \\ \text{no-mixing}, \quad & m_{\tilde{g}} = 200\,\text{GeV}: \quad \Delta_b = 0.06\,, \\ \text{no-mixing}, \quad & m_{\tilde{g}} = 2000\,\text{GeV}: \quad \Delta_b = 0.29\,. \end{aligned} \tag{21}$$

In the no-mixing scenario the A_t value is close to zero, suppressing the $m_{\tilde{g}}$-independent contribution to Δ_b, while the higher SUSY mass scale results in an overall reduction of Δ_b in this scenario. The value of Δ_b in the no-mixing scenario would slightly increase if $m_{\tilde{g}}$ were raised to even larger values, but this effect would not change the qualitative behavior.

Figure 5 shows that the results for the discovery reach in the M_A–$\tan\beta$ plane are relatively stable with respect to variations of the gluino mass. The shift in the discovery contours remains below about $\Delta\tan\beta = 4$ for the $m_h^{\max}$ scenario (left plot) and $\Delta\tan\beta = 1$ for the no-mixing scenario (right plot). For the positive sign of μ chosen in Fig. 5, where the Δ_b correction yields a suppression of the bottom Yukawa coupling, the largest discovery reach is obtained for small $m_{\tilde{g}}$, while the smallest discovery reach is obtained for large $m_{\tilde{g}}$. This behavior would be reversed by a change of sign of μ.

We have also investigated the possible impact of other MSSM parameters (besides μ and $m_{\tilde{g}}$) on the 5σ discovery contours in the M_A–$\tan\beta$ plane. The Δ_b corrections depend also on the parameters in the stop and sbottom sector; see (10). While the formulas in Sect. 2.2.2 have been given for the region where $M_{\text{SUSY}} \gg m_t$, the qualitative effect of reducing the stop and sbottom masses can nevertheless be inferred. Sizable Δ_b corrections require relative large values of μ and $m_{\tilde{g}}$. If these parameters are kept large while the stop and sbottom masses are reduced, the Δ_b corrections tend to decrease. It is obvious from (10) that reducing the absolute value of A_t decreases the electroweak part of the Δ_b correction. As discussed above, this effect of the Δ_b corrections manifests itself in the comparison of the $m_h^{\max}$ and no-mixing scenarios; see Figs. 1–5. Concerning the possible impact of the Δ_b corrections on the 5σ discovery contours for the $b\bar{b}\phi, \phi \to \tau^+\tau^-$ channel in the M_A–$\tan\beta$ plane we conclude that larger effects than those shown in Figs. 1–5 (where we have displayed the discovery contours up to $\tan\beta = 50$) would only arise if the variation of μ were extended over an even wider interval than $-1000\,\text{GeV} \le \mu \le +1000\,\text{GeV}$ as done in our analysis above.

We now turn to the possible effects of other higher-order corrections beyond those entering via Δ_b on the 5σ discovery contours for the $b\bar{b}\phi, \phi \to \tau^+\tau^-$ channel. These effects are in general non-negligible, see the discussions in Sect. 2.2 and in Sect. 4.2 below, but smaller than those induced by Δ_b. As a consequence, the impact on the 5σ discovery contours in the M_A–$\tan\beta$ plane of other supersymmetric parameters entering via higher-order corrections is in general much smaller than the effect of varying μ in the high $\tan\beta$ region of Fig. 4. As an example, the difference observed in Figs. 1–5 between the $m_h^{\max}$ and no-mixing scenarios arising from the different values of A_t and M_{SUSY} in the two scenarios (see (14) and (15)) is mainly an effect of the Δ_b corrections, while the impact of other higher-order corrections involving A_t and M_{SUSY} is found to be small.

Also the decays of the heavy neutral MSSM Higgs bosons into supersymmetric particles are in general affected by other supersymmetric parameters in addition to the dependence on μ, M_A and $\tan\beta$. The resulting effects on $\text{BR}(\phi \to \tau^+\tau^-)$ turn out to be rather small, however. We find that sizable deviations from the values of $\text{BR}(\phi \to \tau^+\tau^-)$ occurring in the $m_h^{\max}$ and no-mixing scenarios for $-1000\,\text{GeV} \le \mu \le +1000\,\text{GeV}$ are only possible in quite extreme regions of the MSSM parameter space that are already highly constrained by existing experimental data.

Our discussion above has been given in the context of the MSSM with real parameters. Since the sensitivity of the 5σ discovery contours in the M_A–$\tan\beta$ plane on the other supersymmetric parameters can mainly be understood as an effect of higher-order corrections to the bottom Yukawa coupling and of the kinematics of Higgs-boson decays into supersymmetric particles, no qualitative changes of our results are expected for the case where complex phases are taken into account.

4.2 Higgs-boson mass precision

The discussion in the previous section shows that the prospective discovery reach of the $b\bar{b}\phi, \phi \to \tau^+\tau^-$ channel in the M_A–$\tan\beta$ plane is rather stable with respect to variations of the other MSSM parameters. We now turn to the second part of our analysis and investigate the expected statistical precision of the Higgs-boson mass measurement. The expected statistical precision is evaluated as described in Sect. 3; see (17). In Figs. 6 and 7 we show the expected precision for the mass measurement achievable from the channel $b\bar{b}\phi, \phi \to \tau^+\tau^-$ using the final states $\tau^+\tau^- \to$ jets and $\tau^+\tau^- \to e+$jet. Within the 5σ discovery region we have indicated contour lines corresponding to different values of the expected precision, $\Delta M/M$. The results are shown in the $m_h^{\max}$ benchmark scenario for $\mu = -200\,\text{GeV}$ (left plots) and $\mu = +200\,\text{GeV}$ (right plots).

We find that experimental precisions of $\Delta M_\phi/M_\phi$ of 1%–4% are reachable within the discovery region. A better precision is reached for larger $\tan\beta$ and smaller M_A as a consequence of the higher number of signal events in this region. The other scenarios and other values of μ discussed above yield qualitatively similar results to those shown in Figs. 6 and 7.

As discussed above, for large values of M_A the heavy neutral MSSM Higgs bosons are nearly mass-degenerate, $M_H \approx M_A$. The experimental separation of the two states H and A (or the corresponding mass eigenstates in the $\mathcal{CP}$-violating case) will therefore be challenging. The results shown in Figs. 6 and 7 have been obtained using the combined sample of H and A events. It is important to note, however, that even in the region of large M_A the mass splitting between M_H and M_H can reach the level of a few %. An example of such a scenario is (as above, we consider the $\mathcal{CP}$-conserving case, i.e. the MSSM with real parameters; the corresponding scenario in the case of non-vanishing complex phases has been discussed in [33])

$$M_{\text{SUSY}} = 500\,\text{GeV}\,,\ A_t = A_b = 1000\,\text{GeV}\,,\ \mu = 1000\,\text{GeV}\,,$$
$$M_2 = 500\,\text{GeV}\,,\ M_1 = 250\,\text{GeV}\,,\ m_{\tilde{g}} = 500\,\text{GeV}\,. \quad (22)$$

In Fig. 8 the mass splitting

$$\frac{\Delta M_{HA}}{M} \equiv \frac{|M_H - M_A|}{\min(M_H, M_A)} \quad (23)$$

is given as a function of X_t for $\tan\beta = 40$ and two M_A values, $M_A = 300\,\text{GeV}$ (solid line) and $M_A = 500\,\text{GeV}$ (dashed line). The dot-dashed and dotted parts of the contours for $M_A = 300, 500\,\text{GeV}$, respectively, in the region of

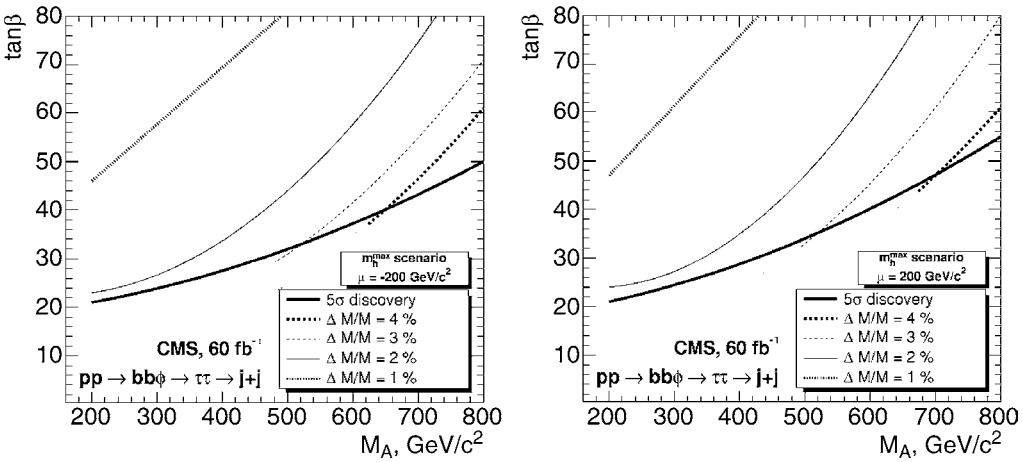

Fig. 6. The statistical precision of the Higgs-boson mass measurement achievable from the channel $b\bar{b}\phi, \phi \to \tau^+\tau^- \to$ jets in the $m_h^{\max}$ benchmark scenario for $\mu = -200\,\text{GeV}$ (*left*) and $\mu = +200\,\text{GeV}$ (*right*) is shown together with the 5σ discovery contour

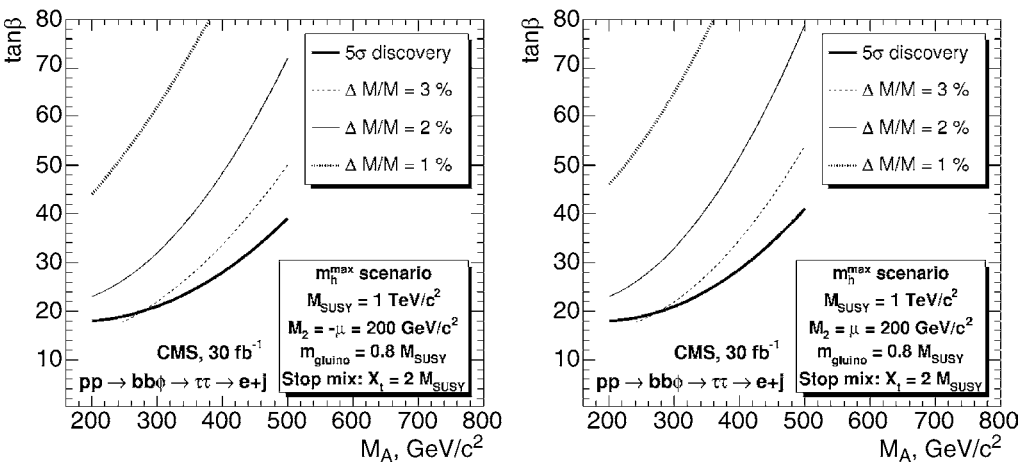

Fig. 7. The statistical precision of the Higgs-boson mass measurement achievable from the channel $b\bar{b}\phi, \phi \to \tau^+\tau^- \to e+$jet in the $m_h^{\max}$ benchmark scenario for $\mu = -200\,\text{GeV}$ (*left*) and $\mu = +200\,\text{GeV}$ (*right*) is shown together with the 5σ discovery contour

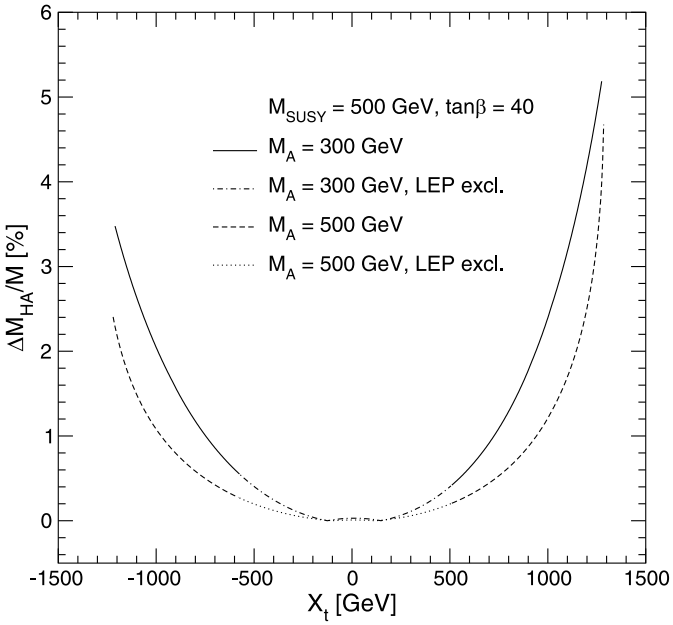

Fig. 8. The mass splitting between the heavy neutral MSSM Higgs bosons, $\Delta M_{HA}/M \equiv |M_H - M_A| / \min(M_H, M_A)$, is shown as a function of X_t for $M_A = 300, 500$ GeV in a scenario with $M_{\rm SUSY} = 500$ GeV, $\mu = 1000$ GeV and $\tan\beta = 40$. The other parameters are given in (22). The *dot-dashed* (*dotted*) parts of the contours for $M_A = 300$ GeV ($M_A = 500$ GeV) indicate parameter combinations that are excluded by the search for the light $\mathcal{CP}$-even Higgs boson of the MSSM at LEP [5]

small $|X_t|$ indicate parameter combinations that result in relatively low M_h values that are excluded by the search for the light $\mathcal{CP}$-even Higgs boson of the MSSM at LEP [5]. One can see in Fig. 8 that the mass splitting between M_H and M_A shows a pronounced dependence on X_t in this scenario. Mass differences of up to 5% are possible for large X_t (while the widths of the Higgs bosons are at the 1%–1.5% level in this parameter region).

The example of Fig. 8 shows that a precise mass measurement at the LHC may in favorable regions of the MSSM parameter space open the exciting possibility to distinguish between the signals of H and A production. In confronting Fig. 8 with the expected accuracies obtained in Figs. 6 and 7 one of course needs to take into account that a separate treatment of the H and A channels in Figs. 6 and 7 would reduce the number of signal events by a factor of 2, resulting in a degradation of the expected accuracies (for the same luminosity) by a factor of $\sqrt{2}$. A more detailed analysis of the potential for experimentally resolving two mass peaks would furthermore have to include effects arising from overlapping Higgs signals. Such an analysis goes beyond the scope of the present paper.

5 Conclusions

We have analyzed the reach of the CMS experiment with 30 or 60 fb^{-1} for the heavy neutral MSSM Higgs bosons, depending on $\tan\beta$ and the Higgs-boson mass scale, M_A. We have focused on the channel $b\bar{b}H/A, H/A \to \tau^+\tau^-$ with the τ subsequently decaying to jets and/or leptons. The experimental analysis, yielding the number of events needed for a 5σ discovery (depending on the mass of the Higgs boson) was performed with full CMS detector simulation and reconstruction for the final states of di-τ-lepton decays. The events were generated with PYTHIA.

The experimental analysis has been combined with predictions for the Higgs-boson masses, production processes and decay channels obtained with the code FeynHiggs, taking into account all relevant higher-order corrections as well as possible decays of the heavy Higgs bosons into supersymmetric particles. We have analyzed the sensitivity of the 5σ discovery contours in the M_A–$\tan\beta$ plane to variations of the other supersymmetric parameters. We have shown that the discovery contours are relatively stable with respect to the impact of additional parameters. The biggest effects, resulting from higher-order corrections to the bottom Yukawa coupling and from the kinematics of Higgs decays into charginos and neutralinos, are caused by varying the absolute value and the sign of the higgsino mass parameter μ. The corresponding shift in the 5σ discovery contours amounts up to about $\Delta\tan\beta = 10$. The effects of other contributions to the relation between the bottom-quark mass and the bottom Yukawa coupling, arising from the gluino mass and the parameters in the stop and sbottom sector, are in general smaller than the shifts induced by a variation of μ. The same holds for the impact of higher-order contributions beyond the corrections to the bottom Yukawa coupling and for the possible effects of other decay modes of the heavy Higgs bosons into supersymmetric particles. The results of our analysis, which was carried out in the framework of the $\mathcal{CP}$-conserving MSSM, should not be substantially affected by the inclusion of complex phases of the soft-breaking parameters.

We have analyzed the prospective accuracy of the mass measurement of the heavy neutral MSSM Higgs bosons in the channel $b\bar{b}H/A, H/A \to \tau^+\tau^-$. We find that statistical experimental precisions of 1%–4% are reachable within the discovery region. These results, obtained from a simple estimate of the prospective accuracies, are not expected to considerably degrade if further uncertainties related to background effects and jet and missing $E_{\rm T}$ scales are taken into account. We have pointed out that a %-level precision of the mass measurements could in favorable regions of the MSSM parameter allow one to experimentally resolve the signals of the two heavy MSSM Higgs bosons.

Acknowledgements. S.H. and G.W. thank M. Carena and C.E.M. Wagner for collaboration on some of the theoretical aspects employed in this analysis.

References

1. H. Nilles, Phys. Rep. **110**, 1 (1984)
2. H. Haber, G. Kane, Phys. Rep. **117**, 75 (1985)
3. R. Barbieri, Riv. Nuovo Cimento **11**, 1 (1988)

4. LEP Higgs working group, Phys. Lett. B **565**, 61 (2003) [hep-ex/0306033]
5. LEP Higgs working group, Eur. Phys. J. C **47**, 547 (2006) [hep-ex/0602042]
6. D0 Collaboration, V. Abazov et al., Phys. Rev. Lett. **95**, 151 801 (2005) [hep-ex/0504018]
7. D0 Collaboration, Phys. Rev. Lett. **97**, 121 802 (2006) [hep-ex/0605009]
8. D0 Collaboration, D0 Note 5331-CONF
9. CDF Collaboration, A. Abulencia et al., Phys. Rev. Lett. **96**, 011 802 (2006) [hep-ex/0508051]
10. CDF Collaboration, CDF note 8676
11. CDF Collaboration, A. Abulencia et al., Phys. Rev. Lett. **96**, 042 003 (2006) [hep-ex/0510065]
12. R. Eusebi, Ph.d. thesis: "Search for charged Higgs in $t\bar{t}$ decay products from proton-antiproton collisions at $\sqrt{s} = 1.96$ TeV" (University of Rochester, 2005)
13. ATLAS Collaboration, Detector and Physics Performance Technical Design Report, CERN/LHCC/99-15 (1999), atlasinfo.cern.ch/Atlas/GROUPS/PHYSICS/TDR/access.html
14. K. Cranmer, Y. Fang, B. Mellado, S. Paganis, W. Quayle, S. Wu, hep-ph/0401148
15. CMS Physics Technical Design Report, Vol. 2. CERN/LHCC 2006-021, cmsdoc.cern.ch/cms/cpt/tdr/
16. V. Büscher, K. Jakobs, Int. J. Mod. Phys. A **20**, 2523 (2005) [hep-ph/0504099]
17. M. Schumacher, Czech. J. Phys. **54**, A103 (2004) [hep-ph/0410112]
18. M. Carena, S. Heinemeyer, C. Wagner, G. Weiglein, hep-ph/9912223
19. M. Carena, S. Heinemeyer, C. Wagner, G. Weiglein, Eur. Phys. J. C **26**, 601 (2003) [hep-ph/0202167]
20. M. Carena, S. Heinemeyer, C. Wagner, G. Weiglein, Eur. Phys. J. C **45**, 797 (2006) [hep-ph/0511023]
21. S. Heinemeyer, W. Hollik, G. Weiglein, JHEP **0006**, 009 (2000) [hep-ph/9909540]
22. A. Belyaev, J. Pumplin, W. Tung, C. Yuan, JHEP **0601**, 069 (2006) [hep-ph/0508222]
23. M. Albrow, A. Rostovtsev, hep-ph/0009336
24. V. Khoze, A. Martin, M. Ryskin, Eur. Phys. J. C **23**, 311 (2002) [hep-ph/0111078]
25. A. De Roeck, V. Khoze, A. Martin, R. Orava, M. Ryskin, Eur. Phys. J. C **25**, 391 (2002) [hep-ph/0207042]
26. B. Cox, AIP Conf. Proc. **753**, 103 (2005) [hep-ph/0409144]
27. J. Forshaw, hep-ph/0508274
28. S. Heinemeyer, V. Khoze, M. Ryskin, W. Stirling, M. Tasevsky, G. Weiglein, arXiv:0708.3052
29. S. Heinemeyer, W. Hollik, G. Weiglein, Comput. Phys. Commun. **124**, 76 (2000) [hep-ph/9812320]
30. S. Heinemeyer, W. Hollik, G. Weiglein, hep-ph/0002213, www.feynhiggs.de
31. S. Heinemeyer, W. Hollik, G. Weiglein, Eur. Phys. J. C **9**, 343 (1999) [hep-ph/9812472]
32. G. Degrassi, S. Heinemeyer, W. Hollik, P. Slavich, G. Weiglein, Eur. Phys. J. C **28**, 133 (2003) [hep-ph/0212020]
33. M. Frank, T. Hahn, S. Heinemeyer, W. Hollik, H. Rzehak, G. Weiglein, JHEP **02**, 047 (2007) [hep-ph/0611326]
34. S. Abdullin et al., Eur. Phys. J. C **39S2**, 41 (2005)
35. R. Kinnunen, A. Nikitenko, CMS note 2003/006
36. J. Thomas, ATL-PHYS-2003-003
37. D. Cavalli, D. Negri, ATL-PHYS-2003-009
38. M. Carena, P. Chankowski, S. Pokorski, C. Wagner, Phys. Lett. B **441**, 205 (1998) [hep-ph/9805349]
39. J. Espinosa, I. Navarro, Nucl. Phys. B **615**, 82 (2001) [hep-ph/0104047]
40. S. Heinemeyer, W. Hollik, G. Weiglein, Phys. Rev. D **58**, 091 701 (1998) [hep-ph/9803277]
41. S. Heinemeyer, Phys. Lett. B **440**, 296 (1998) [hep-ph/9807423]
42. G. Degrassi, A. Dedes, P. Slavich, Nucl. Phys. B **672**, 144 (2003) [hep-ph/0305127]
43. M. Carena, H. Haber, S. Heinemeyer, W. Hollik, C. Wagner, G. Weiglein, Nucl. Phys. B **580**, 29 (2000) [hep-ph/0001002]
44. J. Ellis, G. Ridolfi, F. Zwirner, Phys. Lett. B **257**, 83 (1991)
45. Y. Okada, M. Yamaguchi, T. Yanagida, Prog. Theor. Phys. **85**, 1 (1991)
46. H. Haber, R. Hempfling, Phys. Rev. Lett. **66**, 1815 (1991)
47. A. Brignole, Phys. Lett. B **281**, 284 (1992)
48. P. Chankowski, S. Pokorski, J. Rosiek, Phys. Lett. B **286**, 307 (1992)
49. P. Chankowski, Nucl. Phys. B **423**, 437 (1994) [hep-ph/9303309]
50. A. Dabelstein, Nucl. Phys. B **456**, 25 (1995) [hep-ph/9503443]
51. A. Dabelstein, Z. Phys. C **67**, 495 (1995) [hep-ph/9409375]
52. R. Hempfling, A. Hoang, Phys. Lett. B **331**, 99 (1994) [hep-ph/9401219]
53. J. Casas, J. Espinosa, M. Quirós, A. Riotto, Nucl. Phys. B **436**, 3 (1995)
54. J. Casas, J. Espinosa, M. Quirós, A. Riotto, Nucl. Phys. B **439**, 466 (1995) [hep-ph/9407389]
55. M. Carena, J. Espinosa, M. Quirós, C. Wagner, Phys. Lett. B **355**, 209 (1995) [hep-ph/9504316]
56. M. Carena, M. Quirós, C. Wagner, Nucl. Phys. B **461**, 407 (1996) [hep-ph/9508343]
57. H. Haber, R. Hempfling, A. Hoang, Z. Phys. C **75**, 539 (1997) [hep-ph/9609331]
58. R. Zhang, Phys. Lett. B **447**, 89 (1999) [hep-ph/9808299]
59. J. Espinosa, R. Zhang, JHEP **0003**, 026 (2000) [hep-ph/9912236]
60. G. Degrassi, P. Slavich, F. Zwirner, Nucl. Phys. B **611**, 403 (2001) [hep-ph/0105096]
61. J. Espinosa, R. Zhang, Nucl. Phys. B **586**, 3 (2000) [hep-ph/0003246]
62. A. Brignole, G. Degrassi, P. Slavich, F. Zwirner, Nucl. Phys. B **631**, 195 (2002) [hep-ph/0112177]
63. A. Brignole, G. Degrassi, P. Slavich, F. Zwirner, Nucl. Phys. B **643**, 79 (2002) [hep-ph/0206101]
64. S. Heinemeyer, W. Hollik, H. Rzehak, G. Weiglein, Eur. Phys. J. C **39**, 465 (2005) [hep-ph/0411114]
65. S. Heinemeyer, W. Hollik, H. Rzehak, G. Weiglein, hep-ph/0506254
66. R. Hempfling, Phys. Rev. D **49**, 6168 (1994)
67. L. Hall, R. Rattazzi, U. Sarid, Phys. Rev. D **50**, 7048 (1994) [hep-ph/9306309]
68. M. Carena, M. Olechowski, S. Pokorski, C. Wagner, Nucl. Phys. B **426**, 269 (1994) [hep-ph/9402253]
69. M. Carena, D. Garcia, U. Nierste, C. Wagner, Nucl. Phys. B **577**, 577 (2000) [hep-ph/9912516]
70. H. Eberl, K. Hidaka, S. Kraml, W. Majerotto, Y. Yamada, Phys. Rev. D **62**, 055 006 (2000) [hep-ph/9912463]
71. S. Martin, Phys. Rev. D **65**, 116 003 (2002) [hep-ph/0111209]

72. S. Martin, Phys. Rev. D **66**, 096001 (2002) [hep-ph/0206136]
73. S. Martin, Phys. Rev. D **67**, 095012 (2003) [hep-ph/0211366]
74. S. Martin, Phys. Rev. D **68**, 075002 (2003) [hep-ph/0307101]
75. S. Martin, Phys. Rev. D **70**, 016005 (2004) [hep-ph/0312092]
76. S. Martin, Phys. Rev. D **71**, 016012 (2005) [hep-ph/0405022]
77. S. Martin, Phys. Rev. D **71**, 116004 (2005) [hep-ph/0502168]
78. S. Martin, D. Robertson, Comput. Phys. Commun. **174**, 133 (2006) [hep-ph/0501132]
79. S. Martin, hep-ph/0701051
80. S. Heinemeyer, W. Hollik, G. Weiglein, Phys. Rep. **425**, 265 (2006) [hep-ph/0412214]
81. J. Guasch, P. Häfliger, M. Spira, Phys. Rev. D **68**, 115001 (2003) [hep-ph/0305101]
82. S. Gorishny, A. Kataev, S. Larin, L. Surguladze, Mod. Phys. Lett. A **5**, 2703 (1990)
83. S. Gorishny, Phys. Rev. D **43**, 1633 (1991)
84. A. Kataev, V. Kim, Mod. Phys. Lett. A **9**, 1309 (1994)
85. L. Surguladze, Phys. Lett. B **338**, 229 (1994) [hep-ph/9406294]
86. S. Gorishny, Phys. Lett. B **341**, 60 (1994) [hep-ph/9405325]
87. K. Chetyrkin, Phys. Lett. B **390**, 309 (1997) [hep-ph/9608318]
88. K. Chetyrkin, A. Kwiatkowski, Nucl. Phys. B **461**, 3 (1996) [hep-ph/9505358]
89. S. Larin, T. van Ritbergen, J. Vermaseren, Phys. Lett. B **362**, 134 (1995) [hep-ph/9506465]
90. P. Chankowski, S. Pokorski, J. Rosiek, Nucl. Phys. B **423**, 497 (1994)
91. S. Heinemeyer, W. Hollik, G. Weiglein, Eur. Phys. J. C **16**, 139 (2000) [hep-ph/0003022]
92. R. Harlander, W. Kilgore, Phys. Rev. D **68**, 013001 (2003) [hep-ph/0304035]
93. S. Dittmaier, M. Kramer, M. Spira, Phys. Rev. D **70**, 074010 (2004) [hep-ph/0309204]
94. S. Dawson, C. Jackson, L. Reina, D. Wackeroth, Phys. Rev. D **69**, 074027 (2004) [hep-ph/0311067]
95. Les Houches 2003 Higgs Working Group, K. Assamagan et al., hep-ph/0406152
96. S. Dawson, C. Jackson, L. Reina, D. Wackeroth, Phys. Rev. Lett. **94**, 031802 (2005) [hep-ph/0408077]
97. S. Dawson, C. Jackson, L. Reina, D. Wackeroth, Mod. Phys. Lett. A **21**, 89 (2006) [hep-ph/0508293]
98. J. Campbell, R. Ellis, F. Maltoni, S. Willenbrock, Phys. Rev. D **67**, 095002 (2003) [hep-ph/0204093]
99. A. Martin, R. Roberts, W. Stirling, R. Thorne, Eur. Phys. J. C **28**, 455 (2003) [hep-ph/0211080]
100. T. Hahn, S. Heinemeyer, G. Weiglein, Nucl. Phys. B **652**, 229 (2003) [hep-ph/0211204]
101. people.web.psi.ch/spira/hqq
102. Tevatron Electroweak Working Group, E. Brubaker et al., hep-ex/0608032, tevewwg.fnal.gov/top/
103. Tevatron Electroweak Working Group, hep-ex/0703034
104. OPAL Collaboration, G. Abbiendi et al., Eur. Phys. J. C **35**, 1 (2004) [hep-ex/0401026]
105. S. Gennai, A. Nikitenko, L. Wendland, CMS Note 2006/126
106. R. Kinnunen, S. Lehti, CMS Note 2006/075
107. A. Kalinowski, M. Konecki, D. Kotlinski, CMS Note 2006/105
108. S. Lehti, CMS Note 2006/101
109. T. Sjostrand et al., Comput. Phys. Commun. **135**, 238 (2001) [hep-ph/0010017]
110. J. Campbell, A. Kalinowski, A. Nikitenko, "Comparison between MCFM and Pythia for the $gb \to bh$ and $gg \to b\bar{b}h$ processes at the LHC" in C. Buttar et al., Les Houches Physics at TeVColliders2005, "Standard Model and Higgs working group: Summary report", hep-ph/0604120
111. CompHEP Collaboration, E. Boos et al., Nucl. Instrum. Methods A **534**, 250 (2004) [hep-ph/0403113]